Global Change Biology

WILEY

Global Change Biology

RESEARCH ARTICLE OPEN ACCESS

Reconciling the Discrepancy in Projected Global Dryland Expansion in a Warming World

Sha Zhou[1,2] | Bofu Yu[3]

[1]State Key Laboratory of Earth Surface Processes and Hazards Risk Governance (ESPHR), Faculty of Geographical Science, Beijing Normal University, Beijing, China | [2]Institute of Land Surface System and Sustainable Development, Faculty of Geographical Science, Beijing Normal University, Beijing, China | [3]School of Engineering and Built Environment, Griffith University, Nathan, Queensland, Australia

Correspondence: Sha Zhou (shazhou21@bnu.edu.cn)

Received: 27 August 2024 | **Revised:** 1 February 2025 | **Accepted:** 8 February 2025

Funding: This work was supported by the National Natural Science Foundation of China (42471108), the National Key Research and Development Program of China (2022YFF0801303), and the Fundamental Research Funds for the Central Universities.

Keywords: aridity index | continental dryness | ecohydrological index | global dryland expansion | global warming | hydroclimate changes

ABSTRACT

Continental drying and associated dryland expansion would accelerate environmental degradation and desertification. However, the rate of continental drying commonly assessed with an aridity index is inconsistent with observations and projections of widespread greening and increased global runoff. This raises questions about the accuracy of assessment methods and projections of continental drying and dryland dynamics in a warming world. Here we show that the continental drying trend has been exaggerated because the potential evapotranspiration (PET) and its rate of increase over time are grossly overestimated with the widely used Penman equations. Using an energy-based PET estimator, we bias correct the aridity index and find considerably weaker and less extensive continental drying (47% of the global land area) than the 61%–65% based on Penman equations. Dryland expansion is projected to occur over only 2.1% of global land area in a high-emission scenario in the 21st century. Moreover, the corrected aridity index and ecohydrological and hydroclimate projections all show no change in significance consistently in the extent of global drylands based on 32 climate models. These findings resolve the ongoing debate about global dryland expansion and have far-reaching implications for understanding long-term changes in the climate system and their impacts on terrestrial ecohydrological processes.

1 | Introduction

Continental drying has been observed over much of the Earth's land and is projected to increase in a warmer climate (Greve et al. 2014; Marvel et al. 2019; Cook et al. 2020). This could result in more frequent and more severe droughts, heat waves, and wildfires, and raises serious concerns about the sustainability of ecosystems and our society (Mazdiyasni and AghaKouchak 2015; Abatzoglou and Williams 2016; Zhou, Zhang, et al. 2019; Zhou, Yu, and Zhang 2023). Dryland ecosystems are highly exposed and vulnerable to the warming and drying impacts, which would accelerate environmental degradation and desertification and adversely affect the well-being and livelihood of billions of people (Huang et al. 2017; Song et al. 2024). Further expansion of global drylands in a warmer future would increase the fraction of population affected by water scarcity and land degradation and threaten biodiversity, provision of ecosystem services, and socioeconomic development (Huang et al. 2016; Lian et al. 2021). To protect dryland ecosystems and promote sustainable development, numerous efforts have been made to understand the climate change impacts on continental dryness and the extent of drylands and to develop mitigation and adaptation strategies, including many conservation and restoration programs (Fu et al. 2021; Li et al. 2021).

While past and future dryland changes have been extensively assessed, the magnitude of the continental drying trend and the rate of global dryland expansion remain highly uncertain (Berg and McColl 2021; Feng and Fu 2013; Huang et al. 2016; Lian et al. 2021; Liu et al. 2023; Milly and Dunne 2016). Continental dryness has been commonly evaluated with an aridity index, defined as the ratio of precipitation over the potential evapotranspiration (P/PET), which represents a balance between the water supply at the land surface and the evaporative demand of the atmosphere. Drylands are defined as regions where the aridity index is <0.65 by the United Nations Environment Programme (Middleton and Thomas 1997). The aridity index based on observations and model simulations has shown an enhanced continental drying trend and a persistent expansion of dryland areas since the mid-20th century (Feng and Fu 2013; Huang et al. 2016; Lian et al. 2021). This increase in continental dryness, however, is inconsistent with concomitant increases in global runoff and widespread vegetation greening that indicate ameliorating ecohydrological dryness (Lian et al. 2021; Liu et al. 2023; Piao et al. 2020; Yang et al. 2019; Zhou, Yu, Lintner, Findell, and Zhang 2023). According to an empirical ecohydrological index of aridity based on leaf area index and the relationship between soil moisture and transpiration, no substantial expansion of global drylands is projected to occur even for a high-emission scenario (Berg and McColl 2021). This apparent discrepancy between changes in the aridity index and ecohydrological variables raises questions about the accuracy of the assessment methodology and projections of continental drying and dryland dynamics in a warming world (Greve et al. 2019; McColl et al. 2022; Scheff et al. 2022).

While the concept of dryness or dryland encompasses climatic, hydrological, and ecological characteristics (dry climate, limited water supply, and sparse vegetation; Roderick et al. 2015), dryness essentially implies that water demand well exceeds water supply and could therefore be evaluated with the aridity index (Budyko 1974; Zhou et al. 2015). An important question is whether the ongoing debate over continental drying and dryland expansion originates from the aridity index, particularly an overestimation of the evaporative demand, that is, PET (Greve et al. 2019; Milly and Dunne 2016, 2017; Zhou and Yu 2024). PET is defined as the rate of evapotranspiration (ET) that would occur when the energy supply remains the same but water supply is unlimited, and as such, the PET should be constrained by the net radiation (Milly and Dunne 2016). However, the PET commonly estimated with the Penman equations and especially its rate of increase in future projections have far exceeded those based on the net radiation (Milly and Dunne 2017). This is because the Penman equations incorporate both radiative and aerodynamic controls over the evaporative demand (Penman 1948). When water supply is limited, a lower ET and weaker evaporative cooling would reduce air humidity and increase air temperature, resulting in apparent increases in the evaporative demand associated with aerodynamic conditions to exceed that constrained by the net radiation (Zhou, Williams, et al. 2019; Zhou and Yu 2024). Such overprediction of the PET could be bias corrected using an energy-based approach with the net radiation and a wet Bowen ratio (Zhou and Yu 2024). However, it remains unknown whether the energy-based PET (PET_e) could reconcile the apparent inconsistency between changes in continental dryness and ecohydrological conditions and improve our understanding of the climate change impacts on global dryland expansion.

In this study, the PET_e-based aridity index was used to provide improved projections of continental dryness and dryland dynamics and resolve the discrepancy in global dryland expansion based on climatic, ecohydrological, and hydroclimate changes in a warming world. Observationally constrained ERA5 reanalysis data and historical and future (SSP5-8.5) simulations from 32 global climate models in the Coupled Model Intercomparison Project Phase 6 (CMIP6, Table S1) were used to assess long-term changes in continental dryness and dryland dynamics. The dryland projections using the aridity index (P/PET_e) were combined with those based on the ecohydrological index (Berg and McColl 2021), as well as hydroclimate variables, to provide reliable and consistent projections of global dryland dynamics for a coupled climate–hydrology–ecology system.

2 | Materials and Methods

2.1 | Datasets

ERA5 global reanalysis dataset, that is, the fifth generation reanalysis from the European Centre for Medium-Range Weather Forecasts (ECMWF), uses a high temporal and spatial resolution modeling and data assimilation system, which assimilates a substantial large volume of improved observations to produce a high-quality global reanalysis dataset (Hersbach et al. 2020). By optimally combining observations and model outputs, the ERA5 reanalysis can ensure integrity and coherence in the representation of the global water and energy cycles and ensure the physical consistency between atmospheric and land surface variables for estimating the PET and aridity index. Monthly outputs of total precipitation, ET, surface latent and sensible heat fluxes, air temperature and dew point temperature at 2 m, skin temperature, surface pressure, and wind speed at 10 m for the recent 42 years (1980–2021) were used for this analysis. The net radiation was calculated as the sum of latent and sensible heat fluxes, as ground heat flux is negligible at the monthly scale.

Historical and future simulations from 32 global climate models in CMIP6 (Eyring et al. 2016) were also used for data analysis (Table S1). These models were selected because they have archived all the required monthly outputs as listed for ERA5, except that specific humidity instead of dew point temperature was used in CMIP6. Total runoff was also used to assess changes in the extent of dryland globally. The atmospheric and land surface outputs from the historical (1850–2014) and shared socioeconomic pathway (SSP5-8.5, high emission scenario, 2015–2100) simulations were used to assess past and future changes in the aridity index for the period of 1980–2100. The 32-model ensemble mean was used to filter out the uncertainty from inter-model variability to better represent the land-atmosphere responses to anthropogenic forcings. The projected changes in continental dryness and dryland extent were tested for statistical significance based on the intermodel agreement. To facilitate comparison with ERA5 and CMIP6 models, all data have been resampled to a common spatial resolution of $1° \times 1°$ using the bilinear interpolation method.

To test the consistency between changes in the aridity index and hydroclimate conditions in a warming world, monthly outputs of atmospheric and land surface variables (same as historical and future simulations) from 7 of the 32 CMIP6 models that participated in the 1pctCO2-rad simulations were used (see Section 2.5). In 1pctCO2-rad, CO_2 concentration increases from 285 ppm to 1140 ppm at a rate of 1% per year for 140 years for the atmospheric component only, while the land component is set to a fixed CO_2 concentration of 285 ppm to eliminate the CO_2 physiological effect (i.e., reduced stomatal conductance) on hydroclimate changes. 1pctCO2 simulations have been widely used to assess the CO_2 radiative effect (i.e., climate change) on hydroclimate changes (Scheff et al. 2021; Zhou, Yu, Lintner, Findell, and Zhang 2023).

2.2 | PET Equations

PET is commonly estimated using the Penman equations that involve the radiative and aerodynamic controls over ET (Penman 1948). The open-water Penman equation (PET_{ow}) (Shuttleworth 1993) and the reference crop Penman–Monteith equation (PET_{rc}) (Allen et al. 1998) have been widely adopted to estimate the PET for open water and crop surfaces, respectively.

$$PET_{ow} = \frac{sR_n + 6.43(1 + 0.536u)\gamma VPD}{\lambda(s+\gamma)} \tag{1}$$

$$PET_{rc} = \frac{0.408sR_n + \gamma\frac{900}{T_a+273}uVPD}{s+\gamma(1+0.34u)} \tag{2}$$

where λ is the latent heat of vaporization ($J\,kg^{-1}$); R_n is the net radiation minus ground heat ($J\,m^{-2}\,d^{-1}$), that is, the sum of sensible and latent heat; s is the slope of the curve for saturation vapor pressure with respect to temperature ($Pa\,K^{-1}$); and γ is the psychrometric constant ($Pa\,K^{-1}$). Meteorological variables, including wind speed (u, $m\,s^{-1}$), air temperature (T_a, $^\circ C$), and vapor pressure deficit (VPD, Pa), are observed at 2 m above ground.

The Penman equations above share a common underlying assumption that the evaporative surface is saturated (Penman 1948), which is, however, not satisfied over most land surfaces. For a hypothetical wet surface, the atmospheric conditions that would have adjusted to the condition of such a hypothetical, saturated surface are unknown, and observed/projected meteorological variables over a dry surface have been used to estimate the PET. Therefore, the strong feedbacks of surface (soil) moisture on air temperature, humidity, and wind speed are omitted (Qiao et al. 2023; Zhou et al. 2021, Zhou, Williams, et al. 2019). As suggested by Brutsaert (2015), the estimated PET from the Penman equations with meteorological observations under dry conditions should be called "apparent PET," which is fundamentally different from the PET that would occur when moisture supply is unlimited at the evaporative surface. When the land surface is saturated and coupled with the atmosphere, a larger amount of evaporated water vapor would increase the atmospheric humidity and shift the surface energy partitioning toward evaporative cooling, resulting in a wetter and cooler atmosphere, that is, a lower VPD, and a reduced PET constrained by the net radiation. This suggests that the Penman equations above would overestimate the PET when water supply is limited over land, as demonstrated in previous studies (Greve et al. 2019; Milly and Dunne 2016, 2017; Zhou and Yu 2024).

To resolve the issue above, an energy-based approach has recently been developed to estimate the PET (PET_e) with the net radiation (R_n) and a wet Bowen ratio (β_w) (Zhou and Yu 2024).

$$PET_e = \frac{R_n}{\lambda(1+\beta_w)} \tag{3}$$

PET_e represents the energy limitation to ET, that is, the maximum ET that could occur when the net radiation remains the same, but water supply is unlimited for a hypothetical, saturated surface. β_w is estimated based on the aerodynamics, that is, the ratio of sensible over latent heat exchanged between the saturated surface and the atmosphere.

$$\beta_w = \frac{\gamma(T_s - T_a)}{e_s^* - e_a} \tag{4}$$

where $T_s - T_a$ is the difference between surface (T_s) and air (T_a) temperatures, and $e_s^* - e_a$ is the difference in vapor pressure at the saturated surface (e_s^*) and of the air (e_a) above. As suggested by Zhou and Yu (2024), β_w has two distinct advantages over Penman equations for PET estimation. First, β_w can accurately estimate the Bowen ratio for wet surfaces, allowing PET_e estimated with β_w and R_n to closely match observed/projected ET over the ocean. Second, for dry surfaces, β_w has been demonstrated to be a reliable estimator of the Bowen ratio when the surface becomes saturated. While β_w is estimated using observed/projected meteorological variables under dry conditions, this wet Bowen ratio remains fairly constant due to coupled changes in temperature and humidity of the air and at the land surface from dry to wet conditions (Zhou and Yu 2024). This has resolved the issue of PET overestimation with Penman equations for a dry environment.

Similar to PET_e, another widely used energy-based approach is the Priestley–Taylor equation (PET_{pt}) (Priestley and Taylor 1972), which is a simplified version of the Penman equation, by assuming that the aerodynamic component is approximately 26% of the radiative component ($\frac{sR_n}{s+\gamma}$) for wet surfaces:

$$PET_{pt} = 1.26\frac{sR_n}{\lambda(s+\gamma)} \tag{5}$$

PET_{pt} and PET_e differ in the estimated β_w. Note that PET_{pt} in Equation (5) can be rewritten as

$$PET_{pt} = \frac{R_n}{\lambda\left[1 + \left(0.79\frac{\gamma}{s} - 0.21\right)\right]} \tag{6}$$

It can be seen by comparing Equations (3) and (6) that the equivalent wet Bowen ratio inferred from PET_{pt}, β_{pt}, is a linear function of $\frac{\gamma}{s}$:

$$\beta_{pt} = 0.79\frac{\gamma}{s} - 0.21 \tag{7}$$

which depends on near-surface air temperature only. As β_{pt} in PET_{pt} does not explicitly consider the influence of vertical gradients in temperature and humidity between the land surface and the atmosphere, it tends to overestimate the effect of temperature on surface energy partitioning and varies greatly between dry and wet conditions (Zhou and Yu 2024).

2.3 | Estimation of PET and Aridity Index

The energy-based PET_e and the three Penman equations, that is, PET_{pt}, PET_{ow}, and PET_{rc} were used to estimate the PET. PET_e was estimated with the net radiation and the wet Bowen ratio, that is, Equation (4). Under normal conditions, β_w is larger than zero and smaller than the actual Bowen ratio (β), that is, the ratio of sensible over latent heat, as the land surface is usually unsaturated and the surface temperature is higher than air atmosphere. Occasionally, values of β_w calculated using Equation (4) were found to be negative for some land grid cells, where the surface (skin) temperature is smaller than air temperature at the monthly scale due to the influence of low surface temperature at night. To avoid underestimation of β_w caused by night-time surface temperature, β_w was set to its lower bound based on the relationship between β_w and $\frac{\gamma}{s}$ over the ocean, that is, $\beta_w \geq 0.24 \cdot \frac{\gamma}{s}$ (Zhou and Yu 2024). On the other hand, over snow-covered regions, sensible heat flux can be negative at daytime and therefore negative values of both β_w and β are possible. Thus, β was used as the upper bound for computed β_w using Equation (4). The value of β_w for each month was checked and constrained in sequence as follows: (1) if $\beta_w < 0.24 \cdot \frac{\gamma}{s}$, β_w was set to $0.24 \cdot \frac{\gamma}{s}$; and (2) if $\beta_w > \beta$, β_w was set to β.

PET was calculated at the grid cell and global scales using monthly outputs from ERA5 (1980–2021) and CMIP6 models (1980–2100). At the global scale, the area-weighted mean PET was calculated over land excluding Greenland and Antarctica. The monthly PET was aggregated to the annual scale, along with the annual precipitation, to calculate the aridity index (P/PET) for each year and identify the long-term trend in the aridity index over the period 1980–2100 for each model. Continental drying/wetting trends in the aridity index were evaluated based on the 32-model mean, which was deemed to be robust based on model agreement: the linear trends were significant (p-value <0.05, t-test) and the sign of the significant trends was the same as that of the ensemble mean in at least 22 of the 32 models, which corresponds to a likelihood of 5% by assuming an equal chance of either a positive or negative sign for the significant linear trends across models (Zhou et al. 2022).

To test whether the PET can accurately represent the actual evaporative demand, the PET was compared with the ET over the ocean, where water is abundant and the estimated PET should equal the ET simulated by climate models. Over land, the reliability of the PET (as well as the aridity index) was assessed and validated by examining whether it can be used to reproduce climate model outputs of the runoff ratio based on the Budyko framework (see Section 2.5).

2.4 | Estimation of Global Dryland Areas

Drylands are defined as regions where the aridity index is <0.65, which was adopted by the United Nations Environment Programme (Middleton and Thomas 1997) and widely used in previous studies (Berg and McColl 2021; Feng and Fu 2013; Huang et al. 2016). In this study, this definition was consistently applied to identify the extent of drylands based on different PET equations. The dryland area and its long-term changes were quantified as the fraction over the global land area excluding Greenland and Antarctica; the latter was not included in all analyses to allow a fair comparison with a recent study of dryland dynamics (Berg and McColl 2021). The dryland area for each year in the period of 1980–2100 was computed to identify the spatial and temporal evolution of global drylands and the expansion and/or contraction of global drylands from historical (1991–2020) to future (2071–2100) periods.

The potential changes in global dryland areas were also assessed using the ratio of runoff over precipitation (R/P). As suggested by the Budyko framework (Budyko 1974), the runoff ratio is primarily controlled by climate conditions represented by the aridity index. For each model, an empirical relationship between the runoff ratio and the aridity index across land grid cells in the historical period was established to determine the threshold of the runoff ratio that corresponds to the threshold of 0.65 for the aridity index (Lian et al. 2021). All land grid cells with $P/PET_e < 1.5$ were used to establish the relationship between P/PET_e and R/P. To better capture the nonlinear relationship, different empirical models were attempted, and the quadratic function with the highest determination of coefficient was adopted (Figure S1). A threshold of R/P was determined for each model and used to identify dryland areas for both historical and future periods and to evaluate changes in the fraction of global drylands between the two periods. This method was repeated to identify the threshold of R/P and changes in dryland areas for the three other aridity indexes (P/PET_{pt}, P/PET_{ow}, and PET_{rc}).

2.5 | Projecting the Runoff Ratio From the Aridity Index

To assess the robustness of P/PET_e in reconciling the discrepancy in continental drying, it is essential to determine whether P/PET_e can reliably project changes in the runoff ratio (R/P) in a warming climate (McColl et al. 2022). Although the divergent trends between P/PET_{rc} and R/P can be partly attributed to vegetation physiological responses to elevated CO_2 (Yang et al. 2019), Scheff et al. (2021) show that the divergence remains even when the CO_2 physiological effect is turned off in climate models (i.e., 1pctCO2-rad), likely because of the overestimation of the drying trend by P/PET_{rc}. To explore this further, the relationship between R/P and P/PET can be expressed using the Budyko framework (Yang et al. 2008; Zhou et al. 2016):

$$\frac{R}{P} = 1 - \left[\left(\frac{P}{\mathrm{PET}}\right)^n + 1\right]^{-\frac{1}{n}}, n \in (0, \infty) \quad (8)$$

where the parameter n represents land surface characteristics, such as vegetation, soil, land use, and topographic factors. In a high-emission scenario, the CO_2 physiological effect has been identified as a primary factor responsible for the long-term changes in the parameter n (Zhou, Yu, Lintner, Findell, and Zhang 2023). To isolate the relationship between R/P and P/PET without the CO_2 physiological effect, R/P was estimated from P/PET with a constant parameter n in 1pctCO2-rad, and the estimated R/P was compared with R/P directly obtained from model simulations. For each model/grid cell, the parameter n was first solved based on P/PET and R/P and Equation (8) for the first 30-year period of 1pctCO2-rad, and the value of n for the first 30-year period was used to compute R/P with P/PET and Equation (8) for all subsequent 30-year periods (111 moving averages in total out of the entire 140 years). It is worth noting that while the value of n varies across grid cells, models, and the PET used, it was fixed throughout the entire 140-year period of 1pctCO2-rad for all aridity indexes evaluated to assess their effectiveness in projecting long-term trends in R/P.

3 | Results

3.1 | Long-Term Increases in the Evaporative Demand

The spatial pattern of PET_e from the CMIP6 ensemble is highly consistent with that from ERA5 (Figure 1a,b), with the spatial correlation coefficient (r) of 0.98 for the historical period of 1980–2021 (42 years). The global pattern of PET_e largely resembles that of surface net radiation, with higher values in lower latitudes where the land surface receives and absorbs more solar radiation (Figures 1a,b and S2a,e). PET_e and ET are in close agreement over the ocean, where the mean absolute difference between the two is only 0.4% of the mean ET using ERA5 and 1.4% with the CMIP6 ensemble (Figure S3a,d). This indicates that PET_e accurately represents the evaporative demand under wet conditions.

Over the past 42 years, PET_e increased at a mean rate of 0.78 mm/year over the global land area in ERA5 (Figure 1c). The positive trends over almost all land areas also persist to the end of the 21st century, with a mean trend of 1.1 mm/year during 1980–2100 (Figure 1c,d). The long-term increase in PET_e is mostly attributed to increases in the net radiation over the same period, but is also induced by warming-led reductions in the wet Bowen ratio (β_w), which suggests that a larger fraction of the net radiation is associated with the PET_e if water supply is unlimited (Figures S2i and S4a,f).

Similar to PET_e, both the spatial pattern and long-term trend of PET_{pt} primarily depend on the net radiation (Figure S2). However, PET_{pt} shows higher sensitivity of the Bowen ratio to air temperature and the Bowen ratio inferred from PET_{pt}, that is, β_{pt}, decreases at a rate of −0.074 per century, which is more than twice as large as the rate of −0.028 per century estimated for β_w (Figure S4). This is because β_{pt} is an empirical function of air temperature (Equation 7), and unlike β_w, it does not account for the influence of land-atmosphere gradients of temperature and humidity on surface energy partitioning. Therefore, the long-term trend in PET_{pt}, at a rate of 1.5 mm/year, is 36% higher than that of PET_e for the same period (1980–2100) (Figure S2j,m).

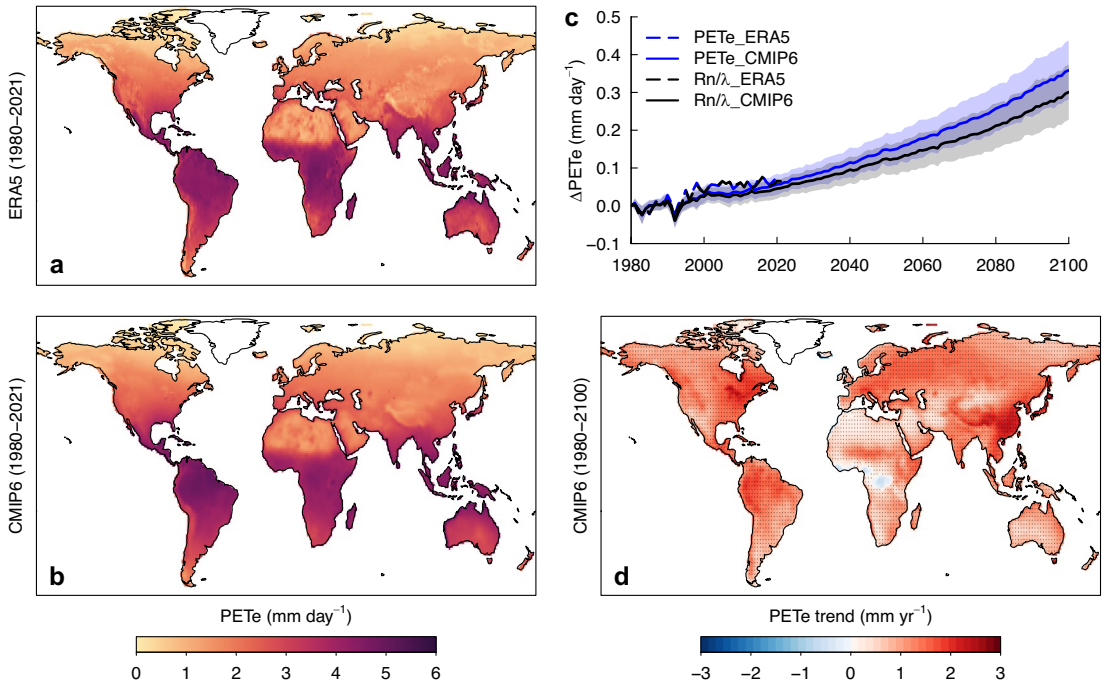

FIGURE 1 | Long-term trends of the potential evapotranspiration (PET) based on ERA5 and CMIP6. (a, b) The energy-based PETe estimated from ERA5 outputs (a) and 32 CMIP6 models (b) during the historical period (1980–2021). (c) Long-term changes in global terrestrial mean annual PET_e and the net radiation (Rn/λ) estimated from ERA5 and CMIP6 based on historical (1980–2014) and future (2015–2100, SSP5-8.5) simulations. The solid lines show multimodel ensemble means, and the shading refers to one standard deviation across the 32 models. (d) Multimodel mean trends in the annual PET_e during 1980–2100 based on CMIP6. Stippling denotes regions where the linear trend is significant (p-value < 0.05) and the sign of the trend is consistent with the sign of the multimodel ensemble mean (as shown in the figure) for at least 22 of the 32 models. Map lines delineate study areas and do not necessarily depict accepted national boundaries.

In contrast to PET_e and PET_{pt}, higher values of PET_{ow} and PET_{rc} occur in mid-latitude dry regions, where lower humidity of the air implies a higher potential for ET, and their values far exceed that constrained by the net radiation (Figure S2). The substantial increases in the annual PET_{ow} and PET_{rc}, both at a rate of 2.37 mm/year for the period 1980–2100, are more than twice the rate of the annual PET_e as projected by the CMIP6 ensemble (Figure S2n,o). In addition to the effect of net radiation, PET_{ow} and PET_{rc} are further increased by higher VPD in a warming climate (Fang et al. 2022), particularly over the Amazon and mid-latitude regions (Figure S2k,l), where precipitation and soil moisture are projected to decline and the reduced ET accelerates warming and drying of the atmosphere, resulting in greater increases in VPD (Cook et al. 2020; Zhou et al. 2022, Zhou, Williams, et al. 2019). Such increases in VPD, and consequently in PET_{ow} and PET_{rc}, are actually a response of the atmosphere to reduced ET, rather than a driving factor forcing ET increases as represented by the evaporative demand.

Compared to the PET_e, the three Penman equations have overestimated the positive trend in the PET with anthropogenic warming over land (Figures 1 and S2). This explains why the long-term increase in PET estimated with the three Penman equations has greatly exceeded that in ET over nonwater-stressed regions (Milly and Dunne 2016). This overestimation may have led to an exaggerated assessment of climate change impacts on continental drying and the apparent discrepancy between changes in continental dryness and ecohydrological and hydroclimate conditions (Berg and McColl 2021; Greve et al. 2019; Huang et al. 2016; Lian et al. 2021; Liu et al. 2023).

3.2 | Reconciling the Discrepancy in Global Dryland Expansion

To address the discrepancy in continental drying, the PET_e-based aridity index (P/PET_e) was used to assess the long-term changes in continental dryness and dryland dynamics, and to compare with those based on the ecohydrological index and hydroclimate changes. The significant decrease (p-value <0.05, t-test) in P/PET_e for at least 22 of the 32 CMIP6 models suggests a robust drying trend over 47% of global land area (Figure 2a, red with stippling), mostly in the Amazon and mid-latitude dry regions, during the period of 1980–2100. The greater increase in PET_e relative to precipitation over 63% of the land area (Figure 2a, red) based on the CMIP6 ensemble corroborates the projected widespread shift from energy to water limitation for terrestrial ET as previously reported (Denissen et al. 2022). Meanwhile, another 25% of the land area (Figure 2a, blue with stippling) is found to experience a significant wetting trend, such as in East

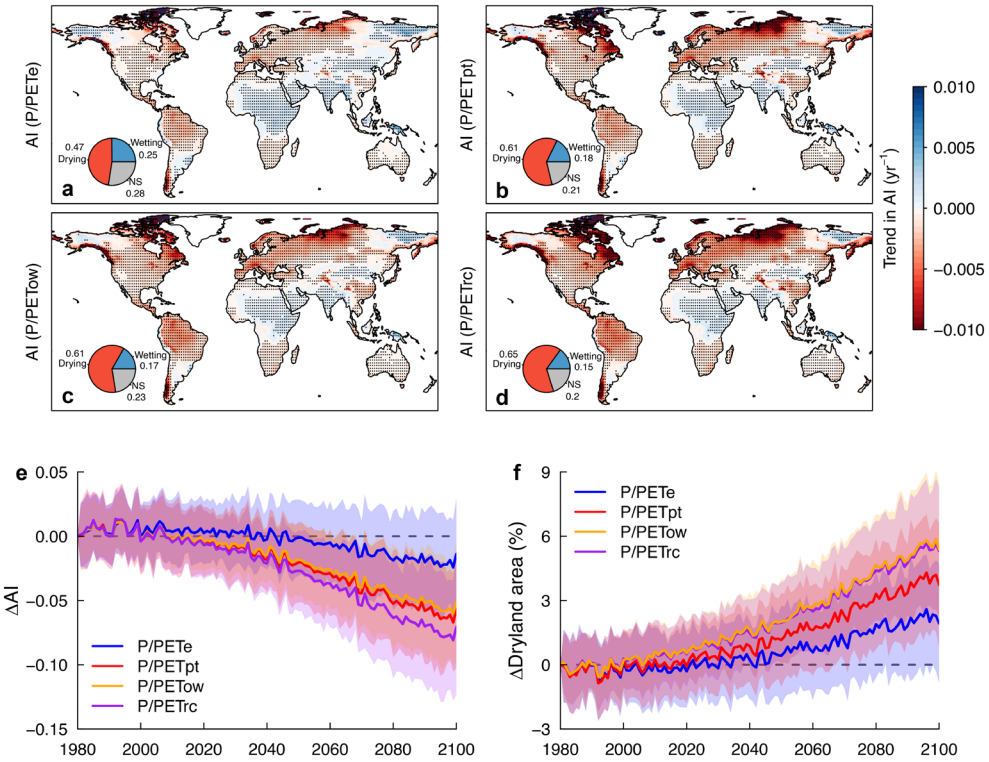

FIGURE 2 | Long-term trends of the aridity index based on CMIP6. (a–d) The multimodel mean trend in the aridity index (AI), that is, the ratio of annual precipitation (P) over the potential evapotranspiration (PET), for the period of 1980–2100. PET was computed with the energy-based PET_e, the Priestley–Taylor equation (PET_{pt}), the open-water Penman equation (PET_{ow}), and the reference crop Penman–Monteith equation (PET_{rc}). Stippling denotes regions where the linear trend is significant (p-value <0.05) and the sign of the trend is consistent with the sign of the multimodel ensemble mean (as shown in the figure) for at least 22 of the 32 CMIP6 models. The pie chart insets show proportions of the land area with (red and blue, stippling) and without (gray, no stippling) significant trends in the aridity index. (e, f) Long-term changes in the global terrestrial mean AI, that is, global mean annual P over global mean annual PET, and the fraction of drylands (AI <0.65) over the global land area, relative to that in 1980. The solid lines show multimodel ensemble means and the shading refers to one standard deviation across the 32 models. Map lines delineate study areas and do not necessarily depict accepted national boundaries.

Africa, India, and North China, where the increase in precipitation has exceeded that in PET_e. The global mean aridity index remains around 0.90 over the historical period 1980–2021 and is projected to decrease to about 0.88 by the end of the 21st century (Figures 2e and S5i). Consistent with this modest drying trend, the dryland area expands by only 0.02% of the global land area per year between 1980 and 2100 (Figures 2f and S5j).

The global dryland area based on the CMIP6 ensemble was compared between historical (1991–2020) and future (2071–2100) periods to identify the spatial extent of dryland expansion and contraction. For the historical period, the fraction and distribution of global drylands identified using P/PET_e align with those using P/PET_{rc}, that is, the aridity index used by the World Atlas of Desertification (Middleton and Thomas 1997) (Figure S5a,g,j), suggesting that P/PET_e is a reliable index for dryland identification. Based on the 32-model mean P/PET_e, global drylands cover 34.6% and 36.7% of the total land area over the historical and future periods, respectively (Figure 3a,b). The expansion and contraction of drylands over 3.3% and 1.2% of the global land area, respectively, occur mostly in the transitional regions between drylands and nondrylands and move toward the regions of long-term decreases and increases in P/PET_e (Figure 3b). The net dryland expansion is identified over only 2.1% of the total land area based on the agreement of at least 22 of the 32 models (Figure S5a,b). However, the difference in the fraction of global drylands between the historical (37.2% ± 4%) and future (39.3% ± 4%) periods is not statistically significant (p-value > 0.05, Figure 3a) based on the 32 models. This assessment of dryland area and its changes is consistent with the finding based on the ecohydrological index (Berg and McColl 2021), which shows that the change in global dryland area is < 1%, from 35.8% during 1971–2000 to 35.1% during 2070–2099 based on 13 CMIP5 models. Moreover, the model spread for the ecohydrological index is much greater (> 30% across 13 models) (Berg and McColl 2021) than that based on P/PET_e (~16% across 32 models, Figure 3a), implying that the ecohydrological index has a much larger amount of uncertainty than the aridity index.

It is worth examining whether the projections of continental dryness and dryland dynamics are consistent with those based on

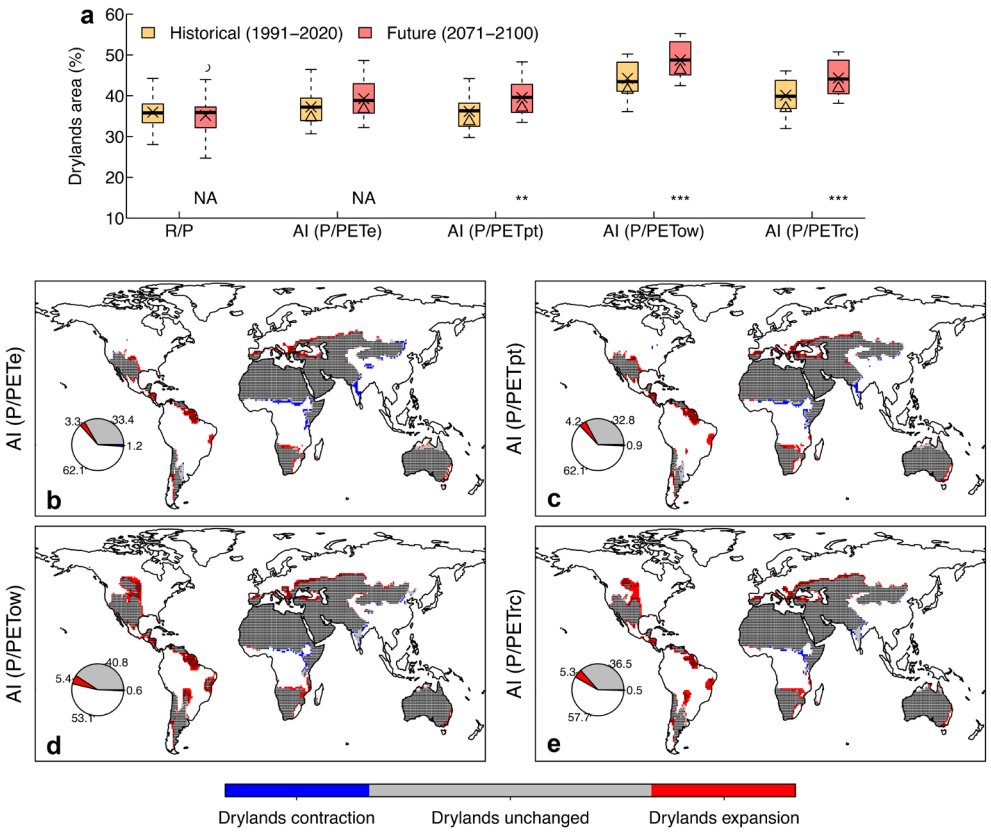

FIGURE 3 | Changes in the total area of global drylands based on CMIP6. (a) Distribution of the global fraction of drylands (AI < 0.65) across the 32 CMIP6 models for the historical (1991–2020) and future (2071–2100) periods, based on the runoff ratio (R/P) and the aridity index (AI) estimated from precipitation and four different PET estimators shown in Figure 2. The threshold of R/P is determined based on the relationship between R/P and P/PET_e for each model (Figure S1). The center line and the cross represent the median and the mean of dryland fractions, respectively, from the 32 models. The triangle represents the dryland fraction estimated based on the mean aridity index from the 32 models. Asterisks below the boxplots indicate the significance level of the difference in dryland area between the two periods (NA for p-value > 0.05, ** for p-value < 0.01, and *** for p-value < 0.001) using the Student's t-test. (b–e) Changes in the spatial extent of drylands between the two periods. The dryland area is identified based on the 32-model mean AI for each period. The pie chart insets show proportions (%) of total land area that experience the expansion (red) and contraction (blue) of drylands. Stippling shows the future area of drylands (AI < 0.65) for at least 22 of the 32 CMIP6 models. Map lines delineate study areas and do not necessarily depict accepted national boundaries.

hydroclimatic variables (i.e., R/P). While the partitioning of precipitation is largely influenced by land surface characteristics, particularly the CO_2 physiological effect, in future simulations (Yang et al. 2019; Zhou, Yu, Lintner, Findell, and Zhang 2023), synchronous changes in P/PET_e and R/P occur over 83% of land grid cells based on the CMIP6 ensemble (81% ± 4% across the 32 models, Figure 4a,f). The Spearman correlation coefficient between changes in P/PET_e and R/P is 0.84 over all land grid cells based on the CMIP6 ensemble (0.82 ± 0.06 across the 32 models, Figure 4a,f). Moreover, the long-term changes in R/P can be effectively reproduced using P/PET_e alone when the CO_2 physiological effect is excluded in 1pctCO2-rad (Figure S6a). Changes in R/P between the first and final 30-year period of 1pctCO2-rad are computed using model outputs and estimated with Equation (8) and P/PET_e, and the global mean difference in these changes of 0.0005 ± 0.0059 is minimal across seven models (Figure S6). This indicates that climatic conditions represented by P/PET_e are tightly correlated and coupled with terrestrial hydrological processes over land.

The fraction of global drylands identified using the R/P threshold is 36.0% ± 4% for the historical period, which is projected to decrease slightly to 35.2% ± 5% for the future period, although this difference is not statistically significant either (p-value > 0.05, Figures 3a and S7) based on the 32 models. When different thresholds (e.g., the aridity index is < 0.6 or 0.7) are used to define drylands, changes in R/P and P/PET_e are still statistically insignificant in terms of the fraction of global drylands between the historical and future periods (p-value > 0.05, Figure S8). These analyses based on climatic, ecohydrological, and hydroclimatic projections consistently show that the expansion of global drylands is insignificant and have resolved the ongoing debate over global dryland expansion in a warming world.

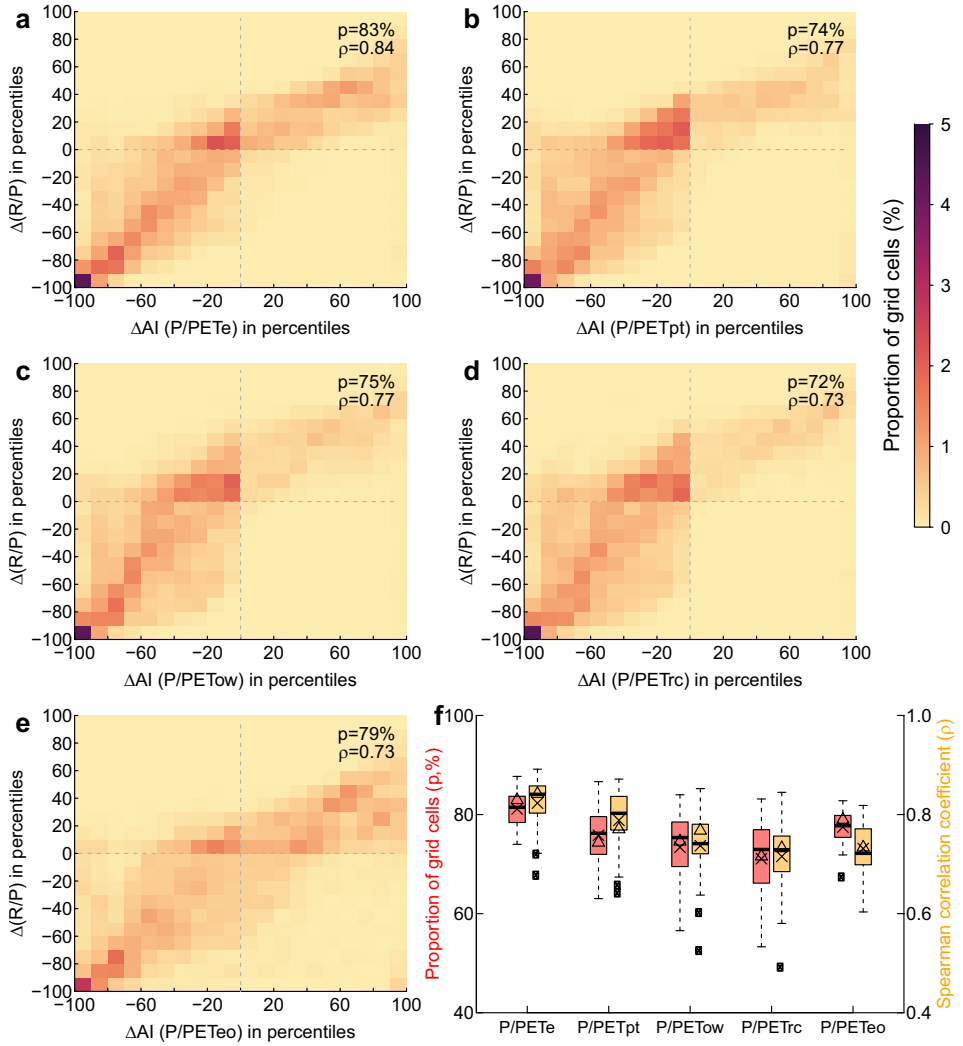

FIGURE 4 | Comparison of changes in the runoff ratio and the aridity index over land. (a–e) Proportion of land grid cells for each percentile bin of 32-model mean changes in the runoff ratio (Δ(R/P) and the aridity index (ΔAI) between the historical (1991–2020) and future (2071–2100) periods. The runoff ratio is calculated with runoff and precipitation directly projected by climate models. The aridity index is estimated from precipitation and four different PET estimators shown in Figure 2 (a–d) and the energy-only PET (PET_{eo}) calculated as 80% of the net radiation (Rn/λ) (e). The y-axis and x-axis show the percentiles for positive and negative Δ(R/P) and ΔAI, respectively. (f) Distributions of the proportion (p, red) of land grid cells having the same direction of Δ(R/P) and ΔAI and the Spearman correlation coefficient (ρ, orange) between Δ(R/P) and ΔAI across land grid cells in the 32 CMIP6 models. The center line and the cross represent the median and the mean of p and ρ from the 32 models, respectively. The triangle in (f) and the top-right numbers in (a–e) show p and ρ estimated using the 32-model mean Δ(R/P) and ΔAI.

3.3 | Exaggeration of Continental Drying Based on Penman Equations

Larger reductions in the aridity index for the drying regions and significant drying trends in larger land areas (61%–65%) were found using the three Penman equations (PET_{pt}, PET_{ow}, and PET_{rc}) in comparison to PET_e (Figure 2). This leads to the apparent discrepancy between the drying trend with the aridity index and a wetting trend suggested by a higher runoff ratio over many areas (Figure 4). In addition, the rate of increase in dryland areas is also greater based on the Penman equations, resulting in a significant expansion of drylands by 4.2%–5.4% of the global land area between the historical and future periods (p-value <0.01, Figure 3). These analyses are consistent with many previous studies (Berg and McColl 2021; Greve et al. 2019; Lian et al. 2021; Liu et al. 2023; Milly and Dunne 2016), indicating that the continental drying and dryland expansion based on the aridity index have been exaggerated, which is caused by the overestimation of PET and its rate of increase over time based on the Penman equations.

To address the exaggeration of continental drying, previous studies suggest using an energy-only equation (PET_{eo}) that is 80% of the net radiation (Milly and Dunne 2017, 2016). It is worth noting that PET_{eo} is a special case of PET_e by assuming a constant β_w value of 0.25 but neglecting its spatial and temporal variations (Figure S4). As a consequence, the temporal and spatial changes in the aridity index and runoff ratio are less consistent using PET_{eo} instead of PET_e, though better than using Penman equations (Figures 4 and S6). In addition, a variant of PET_{rc} that accounts for the elevated CO_2-driven reductions in stomatal resistance (PET_{rc_CO2}) has been invoked to resolve the overestimation of PET_{rc} and the divergent trends between continental dryness and runoff changes (Yang et al. 2019), although their divergence persists in climate model simulations where the vegetation response to elevated CO_2 is turned off (Scheff et al. 2021), as shown in Figure S6a,e. This is because the overestimation of PET_{rc} arises from the elevated VPD coupled with limited soil moisture over dry surfaces (Zhou, Williams, et al. 2019), which remains included in PET_{rc_CO2}. This suggests that only with the PET_e can the overestimation problem of continental drying be resolved satisfactorily in order to reconcile the discrepancy between changes in continental dryness and hydroclimate conditions.

4 | Discussion

In this study, it is shown that the previously identified magnitude and spatial extent of continental drying based on the aridity index, that is, P/PET_{ow} or P/PET_{rc}, are overestimated (Feng and Fu 2013; Huang et al. 2016; Lian et al. 2021). Such an overestimation has manifested itself in the discrepancy between changes in the aridity index and ecohydrological and hydroclimate variables (Figure 4). This overestimation is now confirmed and resolved with P/PET_e. In particular, the consistency in the projected global dryland areas using the aridity index (P/PET_e), the ecohydrological index, and the runoff ratio (R/P) has resolved the ongoing debate over dryland expansion (Berg and McColl 2021; Huang et al. 2016; Lian et al. 2021; Liu et al. 2023) and suggests that the expansion of global drylands is not statistically significant even in a high-emission scenario. These findings also reconcile the apparent inconsistency between changes in climatic, hydrological, and ecological conditions, which are essentially coupled over drylands where water supply is limited. This study provides support for the continued use of the simple aridity index, that is, P/PET_e, as a reliable and meaningful index to capture continental dryness and define drylands in a warming world.

Previous studies have recommended direct assessment of changes in continental dryness based on ecological and hydrological variables, such as vegetation cover, soil moisture, and runoff, rather than relying on simple metrics like the aridity index, as the latter is no longer a reliable proxy for ecohydrological conditions as the climate warms (Greve et al. 2019; McColl et al. 2022; Scheff et al. 2022). This issue has been addressed with P/PET_e, which directly measures the magnitude of water demand relative to water availability and can effectively characterize land surface dryness under both current and future climate conditions. As ecohydrological variables are strongly affected by rising atmospheric CO_2 concentrations and human activities, for example, afforestation, deforestation, urbanization, irrigation, and water abstraction (Lian et al. 2021; Ma et al. 2024; Roderick et al. 2015; Zhou, Yu, Lintner, Findell, and Zhang 2023), they are not directly representative of regional climatic dryness and therefore not suitable for assessment of continental dryness as a result of climate change. That is why the aridity index has been most widely used to define drylands and assess changes in dryness (Huang et al. 2016; Li et al. 2021; Feng and Fu 2013; Milly and Dunne 2016; Liu et al. 2023). Furthermore, projected ecohydrological variables are subject to large amounts of uncertainty, with high intermodel spread of drylands assessment based on the ecohydrological index (Berg and McColl 2021). By comparison, this intermodel spread can be greatly reduced with P/PET_e (Figure 3a).

It is worth noting that PET_e is estimated as the maximum ET that could occur when the water supply at the evaporative surface is unlimited and essentially represents the energy limitation for ET. According to the Budyko hypothesis (Budyko 1974), PET_e can be regarded as an intrinsically important climatic characteristic like precipitation that affects the terrestrial water cycle. This has important implications for estimating ET and projecting its future changes, because the PET sets the upper bound for ET in remote sensing and reanalysis products (Martens et al. 2017; Mu et al. 2011; Zhang et al. 2019) and various hydrological models (Kumar et al. 2017; Zhao et al. 2013; Zhou et al. 2015). In particular, the discrepancy in projected changes in ET and runoff based on the aridity index and directly from climate models, which can be mostly attributed to the overestimation of PET (Milly and Dunne 2016, 2017; Greve et al. 2019), would be greatly reduced or eliminated with PET_e (Figure S6). Given its critical importance, establishing a comprehensive network of ground-based PET observations, particularly at flux towers or meteorological stations, is essential for further validating PET_e. This would enhance the accuracy and reliability of PET estimates, ultimately improving our ability to model and predict water cycle dynamics under a changing climate. Additionally, the terrestrial water cycle is influenced by vegetation responses to the drying trend

and elevated CO_2, which remain highly uncertain in current climate models (Yang et al. 2019; Zhou, Yu, Lintner, Findell, and Zhang 2023). This underscores the need for improved constraints on these processes based on integrated climate, hydrological, and ecological observations. Such advancements would enable more reliable projections of hydrological changes to inform water resources planning and management, especially in water-limited regions.

In summary, this study reconciles the considerable difference in projected changes to global drylands using the aridity index and the ecohydrological index and provides robust evidence to suggest much weaker and less extensive continental drying than previously reported for a warming world. The findings have broader implications for understanding the past and future changes in the climate system and evaluating their impacts on terrestrial hydrological and ecological processes, particularly over drylands that are highly exposed and vulnerable to climate change impacts (Gu et al. 2025; Li et al. 2021; Reynolds et al. 2007). Climate change manifests itself in changes in surface energy balance, that is, coupled changes in temperature and humidity between the land surface and the atmosphere. To evaluate changes in the evaporative demand and the likely drying or wetting of continents, it is essential to consider the energy balance and avoid taking into consideration apparent increases in the evaporative demand due to increases in VPD, which may actually be a response to reduced ET, rather than a control over ET when water supply to the evaporative surface is limited (Qiao et al. 2023; Zhou, Williams, et al. 2019; Zhou and Yu 2024). Moreover, a holistic understanding of continental dryness based on climatic, hydrological, and ecological changes in the coupled land–atmosphere system will better inform adaptation strategies to mitigate the adverse consequences of climate change on natural ecosystems and human well-being.

Author Contributions

Sha Zhou: conceptualization, data curation, formal analysis, funding acquisition, investigation, methodology, project administration, resources, software, validation, visualization, writing – original draft, writing – review and editing. **Bofu Yu:** conceptualization, methodology, writing – review and editing.

Acknowledgments

We acknowledge the World Climate Research Programme's Working Group on Coupled Modelling, which is responsible for CMIP, and we thank the climate modeling groups (listed in Table S1 of this paper) for producing and making available their model output. For CMIP, the U.S. Department of Energy's Program for Climate Model Diagnosis and Intercomparison provides coordinating support and led the development of software infrastructure in partnership with the Global Organization for Earth System Science Portals. We also acknowledge the Copernicus Climate Change Service, which is operated by the ECMWF on behalf of the European Union, for generating and distributing the ERA5 reanalysis dataset (https://doi.org/10.24381/cds.f17050d7). This work was supported by the National Natural Science Foundation of China (42471108), the National Key Research and Development Program of China (2022YFF0801303), and the Fundamental Research Funds for the Central Universities.

Conflicts of Interest

The authors declare no conflicts of interest.

Data Availability Statement

The data that support the findings of this study are openly available in Zenodo at https://doi.org/10.5281/zenodo.14865506. The ERA5 reanalysis product from the European Centre for Medium-Range Weather Forecasts (ECMWF) was obtained from the Copernicus Climate Change Service (C3S) Climate Data Store (CDS) at https://doi.org/10.24381/cds.f17050d7. Information on the CMIP6 model simulations used in this study can be found in Table S1.

References

Abatzoglou, J. T., and A. P. Williams. 2016. "Impact of Anthropogenic Climate Change on Wildfire Across Western US Forests." *Proceedings of the National Academy of Sciences of the United States of America* 113: 11770–11775. https://doi.org/10.1073/pnas.1607171113.

Allen, R. G., L. S. Pereira, D. Raes, and M. Smith. 1998. *Crop Evapotranspiration: Guidelines for Computing Crop Water Requirements, FAO Irrigation and Drainage Paper.* Food and Agriculture Organization of the United Nations.

Berg, A., and K. A. McColl. 2021. "No Projected Global Drylands Expansion Under Greenhouse Warming." *Nature Climate Change* 11: 331–337. https://doi.org/10.1038/s41558-021-01007-8.

Brutsaert, W. 2015. "A Generalized Complementary Principle With Physical Constraints for Land-Surface Evaporation." *Water Resources Research* 51: 8087–8093. https://doi.org/10.1002/2015WR017720.

Budyko, M. I. 1974. *Climate and Life, International Geophysics Series.* Academic Press.

Cook, B. I., J. S. Mankin, K. Marvel, A. P. Williams, J. E. Smerdon, and K. J. Anchukaitis. 2020. "Twenty-First Century Drought Projections in the CMIP6 Forcing Scenarios." *Earth's Future* 8: e2019EF001461. https://doi.org/10.1029/2019EF001461.

Denissen, J. M. C., A. J. Teuling, A. J. Pitman, et al. 2022. "Widespread Shift From Ecosystem Energy to Water Limitation With Climate Change." *Nature Climate Change* 12: 677–684. https://doi.org/10.1038/s41558-022-01403-8.

Eyring, V., S. Bony, G. A. Meehl, et al. 2016. "Overview of the Coupled Model Intercomparison Project Phase 6 (CMIP6) Experimental Design and Organization." *Geoscientific Model Development* 9: 1937–1958. https://doi.org/10.5194/gmd-9-1937-2016.

Fang, Z., W. Zhang, M. Brandt, A. M. Abdi, and R. Fensholt. 2022. "Globally Increasing Atmospheric Aridity Over the 21st Century." *Earth's Future* 10: e2022EF003019. https://doi.org/10.1029/2022EF003019.

Feng, S., and Q. Fu. 2013. "Expansion of Global Drylands Under a Warming Climate." *Atmospheric Chemistry and Physics* 13: 10081–10094. https://doi.org/10.5194/acp-13-10081-2013.

Fu, B., M. Stafford-Smith, Y. Wang, et al. 2021. "The Global-DEP Conceptual Framework – Research on Dryland Ecosystems to Promote Sustainability." *Current Opinion in Environmental Sustainability* 48: 17–28. https://doi.org/10.1016/j.cosust.2020.08.009.

Greve, P., B. Orlowsky, B. Mueller, J. Sheffield, M. Reichstein, and S. I. Seneviratne. 2014. "Global Assessment of Trends in Wetting and Drying Over Land." *Nature Geoscience* 7: 716–721. https://doi.org/10.1038/ngeo2247.

Greve, P., M. L. Roderick, A. M. Ukkola, and Y. Wada. 2019. "The Aridity Index Under Global Warming." *Environmental Research Letters* 14: 124006. https://doi.org/10.1088/1748-9326/ab5046.

Gu, B., S. Zhou, B. Yu, K. L. Findell, and B. R. Lintner. 2025. "Multifaceted Changes in Water Availability With a Warmer Climate." *NPJ Climate and Atmospheric Science* 8: 31. https://doi.org/10.1038/s41612-025-00913-4.

Hersbach, H., B. Bell, P. Berrisford, et al. 2020. "The ERA5 Global Reanalysis." *Quarterly Journal of the Royal Meteorological Society* 146: 1999–2049. https://doi.org/10.1002/qj.3803.

Huang, J., Y. Li, C. Fu, et al. 2017. “Dryland Climate Change: Recent Progress and Challenges.” *Reviews of Geophysics* 55: 719–778. https://doi.org/10.1002/2016RG000550.

Huang, J., H. Yu, X. Guan, G. Wang, and R. Guo. 2016. “Accelerated Dryland Expansion Under Climate Change.” *Nature Climate Change* 6: 166–171. https://doi.org/10.1038/nclimate2837.

Kumar, S. V., S. Wang, D. M. Mocko, C. D. Peters-Lidard, and Y. Xia. 2017. “Similarity Assessment of Land Surface Model Outputs in the North American Land Data Assimilation System.” *Water Resources Research* 53: 8941–8965. https://doi.org/10.1002/2017WR020635.

Li, C., B. Fu, S. Wang, et al. 2021. “Drivers and Impacts of Changes in China's Drylands.” *Nature Reviews Earth and Environment* 2: 858–873. https://doi.org/10.1038/s43017-021-00226-z.

Lian, X., S. Piao, A. Chen, et al. 2021. “Multifaceted Characteristics of Dryland Aridity Changes in a Warming World.” *Nature Reviews Earth and Environment* 2: 232–250. https://doi.org/10.1038/s43017-021-00144-0.

Liu, Z., T. Wang, and H. Yang. 2023. “Overestimated Global Dryland Expansion With Substantial Increases in Vegetation Productivity Under Climate Warming.” *Environmental Research Letters* 18: 054024. https://doi.org/10.1088/1748-9326/accfb1.

Ma, S., S. Zhou, B. Yu, and J. Song. 2024. “Deforestation-Induced Runoff Changes Dominated by Forest-Climate Feedbacks.” *Science Advances* 10: eadp3964.

Martens, B., D. Gonzalez Miralles, H. Lievens, et al. 2017. “GLEAM v3: Satellite-Based Land Evaporation and Root-Zone Soil Moisture.” *Geoscientific Model Development* 10: 1903–1925. https://doi.org/10.5194/gmd-10-1903-2017.

Marvel, K., B. I. Cook, C. J. W. Bonfils, P. J. Durack, J. E. Smerdon, and A. P. Williams. 2019. “Twentieth-Century Hydroclimate Changes Consistent With Human Influence.” *Nature* 569: 59–65. https://doi.org/10.1038/s41586-019-1149-8.

Mazdiyasni, O., and A. AghaKouchak. 2015. “Substantial Increase in Concurrent Droughts and Heatwaves in the United States.” *Proceedings of the National Academy of Sciences of the United States of America* 112: 11484–11489. https://doi.org/10.1073/pnas.1422945112.

McColl, K. A., M. L. Roderick, A. Berg, and J. Scheff. 2022. “The Terrestrial Water Cycle in a Warming World.” *Nature Climate Change* 12: 604–606. https://doi.org/10.1038/s41558-022-01412-7.

Middleton, N., and D. Thomas. 1997. *World Atlas of Desertification*. 2nd ed. Wiley.

Milly, P. C. D., and K. A. Dunne. 2016. “Potential Evapotranspiration and Continental Drying.” *Nature Climate Change* 6: 946–949. https://doi.org/10.1038/nclimate3046.

Milly, P. C. D., and K. A. Dunne. 2017. “A Hydrologic Drying Bias in Water-Resource Impact Analyses of Anthropogenic Climate Change.” *JAWRA Journal of the American Water Resources Association* 53: 822–838. https://doi.org/10.1111/1752-1688.12538.

Mu, Q., M. Zhao, and S. W. Running. 2011. “Improvements to a MODIS Global Terrestrial Evapotranspiration Algorithm.” *Remote Sensing of Environment* 115: 1781–1800. https://doi.org/10.1016/j.rse.2011.02.019.

Penman, H. L. 1948. “Natural Evaporation From Open Water, Bare Soil and Grass.” *Proceedings of the Royal Society of London. Series A: Mathematical and Physical Sciences* 192: 120–145.

Piao, S., X. Wang, T. Park, et al. 2020. “Characteristics, Drivers and Feedbacks of Global Greening.” *Nature Reviews Earth and Environment* 1: 14–27. https://doi.org/10.1038/s43017-019-0001-x.

Priestley, C. H. B., and R. J. Taylor. 1972. “On the Assessment of Surface Heat Flux and Evaporation Using Large-Scale Parameters.” *Monthly Weather Review* 100: 81–92.

Qiao, L., Z. Zuo, R. Zhang, S. Piao, D. Xiao, and K. Zhang. 2023. “Soil Moisture–Atmosphere Coupling Accelerates Global Warming.” *Nature Communications* 14: 4908. https://doi.org/10.1038/s41467-023-40641-y.

Reynolds, J. F., D. M. S. Smith, E. F. Lambin, et al. 2007. “Global Desertification: Building a Science for Dryland Development.” *Science* 316: 847–851. https://doi.org/10.1126/science.1131634.

Roderick, M. L., P. Greve, and G. D. Farquhar. 2015. “On the Assessment of Aridity With Changes in Atmospheric CO_2.” *Water Resources Research* 51: 5450–5463. https://doi.org/10.1002/2015WR017031.

Scheff, J., S. Coats, and M. M. Laguë. 2022. “Why Do the Global Warming Responses of Land-Surface Models and Climatic Dryness Metrics Disagree?” *Earth's Future* 10: e2022EF002814. https://doi.org/10.1029/2022EF0028148.

Scheff, J. S., J. Mankin, S. Coats, and H. Liu. 2021. “CO_2-Plant Effects Do Not Account for the Gap Between Dryness Indices and Projected Dryness Impacts in CMIP6 or CMIP5.” *Environmental Research Letters* 16: 034018. https://doi.org/10.1088/1748-9326/abd8fd.

Shuttleworth, W. J. 1993. *Handbook of Hydrology*. McGraw-Hill Education.

Song, J., S. Zhou, B. Yu, et al. 2024. “Serious Underestimation of Reduced Carbon Uptake due to Vegetation Compound Droughts.” *NPJ Climate and Atmospheric Science* 7: 23. https://doi.org/10.1038/s41612-024-00571-y.

Yang, H., D. Yang, Z. Lei, and F. Sun. 2008. “New Analytical Derivation of the Mean Annual Water-Energy Balance Equation.” *Water Resources Research* 44: 893–897. https://doi.org/10.1029/2007WR0061353.

Yang, Y., M. L. Roderick, S. Zhang, T. R. McVicar, and R. J. Donohue. 2019. “Hydrologic Implications of Vegetation Response to Elevated CO_2 in Climate Projections.” *Nature Climate Change* 9: 44–48. https://doi.org/10.1038/s41558-018-0361-0.

Zhang, Y., D. Kong, R. Gan, et al. 2019. “Coupled Estimation of 500 m and 8-Day Resolution Global Evapotranspiration and Gross Primary Production in 2002–2017.” *Remote Sensing of Environment* 222: 165–182. https://doi.org/10.1016/j.rse.2018.12.031.

Zhao, L., J. Xia, C. Xu, Z. Wang, L. Sobkowiak, and C. Long. 2013. “Evapotranspiration Estimation Methods in Hydrological Models.” *Journal of Geographical Sciences* 23: 359–369. https://doi.org/10.1007/s11442-013-1015-9.

Zhou, S., A. P. Williams, A. M. Berg, et al. 2019. “Land–Atmosphere Feedbacks Exacerbate Concurrent Soil Drought and Atmospheric Aridity.” *Proceedings of the National Academy of Sciences of the United States of America* 116: 18848–18853. https://doi.org/10.1073/pnas.1904955116.

Zhou, S., A. P. Williams, B. R. Lintner, et al. 2021. “Soil Moisture–Atmosphere Feedbacks Mitigate Declining Water Availability in Drylands.” *Nature Climate Change* 11: 38–44. https://doi.org/10.1038/s41558-020-00945-z.

Zhou, S., A. P. Williams, B. R. Lintner, et al. 2022. “Diminishing Seasonality of Subtropical Water Availability in a Warmer World Dominated by Soil Moisture–Atmosphere Feedbacks.” *Nature Communications* 13: 5756. https://doi.org/10.1038/s41467-022-33473-9.

Zhou, S., and B. Yu. 2024. “Physical Basis of the Potential Evapotranspiration and Its Estimation Over Land.” *Journal of Hydrology* 641: 131825. https://doi.org/10.1016/j.jhydrol.2024.131825.

Zhou, S., B. Yu, Y. Huang, and G. Wang. 2015. “The Complementary Relationship and Generation of the Budyko Functions.” *Geophysical Research Letters* 42: 1781–1790. https://doi.org/10.1002/2015GL063511.

Zhou, S., B. Yu, B. R. Lintner, K. L. Findell, and Y. Zhang. 2023. “Projected Increase in Global Runoff Dominated by Land Surface Changes.” *Nature Climate Change* 13: 442–449. https://doi.org/10.1038/s41558-023-01659-8.

Zhou, S., B. Yu, L. Zhang, Y. Huang, M. Pan, and G. Wang. 2016. “A New Method to Partition Climate and Catchment Effect on the Mean

Annual Runoff Based on the Budyko Complementary Relationship." *Water Resources Research* 52: 7163–7177. https://doi.org/10.1002/2016WR019046.

Zhou, S., B. Yu, and Y. Zhang. 2023. "Global Concurrent Climate Extremes Exacerbated by Anthropogenic Climate Change." *Science Advances* 9: eabo163810. https://doi.org/10.1126/sciadv.abo1638.

Zhou, S., Y. Zhang, A. P. Williams, and P. Gentine. 2019. "Projected Increases in Intensity, Frequency, and Terrestrial Carbon Costs of Compound Drought and Aridity Events." *Science Advances* 5: eaau5740. https://doi.org/10.1126/sciadv.aau5740.

Supporting Information

Additional supporting information can be found online in the Supporting Information section.